Cold rolling of foil

N A Fleck, BA, MA, PhD, **K L Johnson,** FRS, MA, PhD, FEng, FIMechE
M E Mear, BS, SM, PhD and **L C Zhang,** BSc, PhD, MEng
Department of Engineering, University of Cambridge

A theory of cold rolling of thin gauge strip is presented which, within the idealizations of homogeneous deformation and a constant coefficient of Coulomb friction, rigorously models the elastic deformation of the rolls and the frictional traction at the interface. In contrast with classical theories (3) *it is shown that, for gauges less than a critical value, plastic reduction takes place in two zones, at entry and exit, which are separated by a neutral zone in which the rolls are compressed flat and there is no slip between the rolls and the strip. Roll load and torque are governed by five independent non-dimensional parameters which express the influence of gauge, reduction, friction and front and back tensions. Values of load and torque have been computed (for zero front and back tensions) for a wide range of thickness, reduction and friction and have been found to collapse approximately on to a single master curve.*

NOTATION

a	contact width from centre-line of rolls to entry or exit location
b	semi-thickness of strip
B	non-dimensional strip semi-thickness = bE_R^{*2}/RY_s^2
c	semi-length of overlapping triangular element
C_{ij}, D_{ij}	influence matrices for normal displacement of rolls
C'_{ij}, D'_{ij}	influence matrices for displacement gradient $\partial u/\partial x$ of rolls
E	Young modulus
E^*	plane strain Young modulus = $E/(1-\nu^2)$
h	thickness of strip
I, K	integrals (Appendix 3)
$J(x)$	Cauchy integral of $q = \int_{-a_0}^{a_2} \{q(x')/(x-x')\}\,dx'$
l	contact length of strip in nip
m	friction factor = $2q/Y_s$
p, q	normal pressure and shear stress, respectively, between rolls and strip
P	non-dimensional pressure = p/Y_s
Q	roll torque per work roll, per unit width of strip
$\bar{Q}$	non-dimensional roll torque = $QE_R^{*2}/R^2Y_s^3$
r	overall reduction of strip = $(b_0 - b_2)/b_0$
R	radius of undeformed work roll
u, v	tangential and normal displacements, respectively
U	non-dimensional group for $\mu = \mu E_R^*/Y_s$
V	velocity of unstrained strip or rolls in x direction
W	roll load per unit width of strip
$\bar{W}$	non-dimensional roll load = WE_R^*/RY_s^2
x, z	Cartesian coordinates
X	non-dimensional coordinate in x direction = xE_R^*/RY_s
Y_s	plane strain yield stress of strip
α	factor describing direction of friction = $q/\|q\| = \pm 1$
ε	tensile strain in longitudinal x direction
μ	coefficient of Coulomb friction
ν	Poisson ratio
ξ	creep coefficient = $(V_S - V_R)/V_R$
ξ, ξ_1	coordinates (in Appendix 3)
σ	tensile direct stress in strip
Σ	non-dimensional front or back tension on strip = σ/Y_s
τ	shear stress

Subscripts

c	critical
i, j, k	integers
p	peak
A, B, C, D, E, F	zones of deformation
S	strip
R	work roll
0	quantity at entry of strip into roll bite
1	quantity in the central, no-slip zone
2	quantity at exit of strip from roll bite

Superscripts

e	elastic
p	plastic
–	average
·	rate

The MS was received on 6 June 1991 and was accepted for publication on 15 January 1992.

1 INTRODUCTION

Conventional theories of cold rolling such as those developed by von Karmann (**1**), Orowan (**2**) and Bland and Ford (**3**) are known to be unsatisfactory for describing the process of rolling thin hard strip or foil. They either neglect elastic deformation of the rolls or assume that their deformed profile remains a circular arc of enlarged radius given by the Hitchcock formula (**4**). A further assumption of these theories is that the plastic deformation of the strip is 'homogeneous', that is plane cross-sections remain plane throughout the bite. It follows from these two assumptions that plastic reduction of the strip is continuous through the bite apart from small arcs of elastic compression at entry

0954-4054/92 $3.00 + .05

and recovery at exit. The strip slips relative to the rolls everywhere except at the 'neutral point' (or section) where the slip direction changes from backwards at entry to forwards at exit.

When applied to thin gauges these theories [for example reference (3)] suggest that there is a limiting gauge below which reduction cannot be achieved; increasing the roll load flattens the rolls elastically without causing yield of the strip. This proposition was investigated by Johnson and Bentall (5) and was found to be false as, indeed, the industrial production of foil down to 0.020 mm gauge clearly demonstrates. The fallacy in the theory lies in the assumption that slip occurs, and hence limiting friction is sustained, throughout the bite. Johnson and Bentall (5) considered the onset of plastic reduction of a thin elastic strip between two rolls. They showed that, with increasing roll load, yielding of the strip initiates at two well-separated points, one close to entry and the other close to exit. This result strongly suggests that if the roll load is further increased so that plastic reduction of the strip occurs, it will take place in two zones, one at entry and the other at exit, separated by an extensive neutral zone. In the neutral zone there is no slip between the strip and the rolls, and the frictional traction does not reach its limiting value.

This suggestion was explored by Fleck and Johnson (6) in an analysis of foil rolling in which the elastic deformation of the rolls was modelled by an elastic foundation—the 'mattress model'. This approximate analysis gave strong support for the hypothesis that reduction in foil rolling takes place in two zones, one at entry and the other at exit, separated by an extensive neutral zone.

In this paper the mattress model has been abandoned and the rolls are modelled by elastic half-spaces. As in the Hertz theory, this is a good approximation provided the length of the contact zone is small compared with the radius of the rolls, a condition well met in foil rolling. An analysis of strip rolling which models the deformation of the rolls in this way has been presented by Grimble and co-workers (7, 8). Unfortunately, through not recognizing the possibility of a no-slip zone, Grimble and co-workers assumed that the frictional traction takes its limiting value throughout the bite.

Modern developments in modelling the rolling of thicker gauges use finite element methods to avoid the simplification of homogeneous plastic deformation of the strip. The errors involved in this simplification, which effectively averages stresses through the thickness of the strip, generally decrease with decreasing thickness of the strip compared with the length of the bite. It seems justifiable, therefore, to retain the assumption of homogeneous deformation of the strip; its influence will be discussed later.

The most significant unknown quantity in the process is the friction between the rolls and strip. Its importance in foil rolling is revealed both by analysis and by the practical observation that the reduction obtained at a given load increases with rolling speed through improved lubrication. The difficulties of predicting the friction arise from the necessity of working in the 'mixed' lubrication regime which is in part hydrodynamic and in part boundary. In this phase of the project the coefficient of friction μ is taken to be constant, while recognizing that its value may depend upon speed and surface conditions.

Finally, the results presented here will be for an elastic-perfectly plastic strip (plane strain yield stress Y_s = constant) and for zero front and back tensions (stresses).

2 FORM OF THE SOLUTIONS

Before proceeding to the analysis, it is instructive to examine qualitatively a set of solutions for the pressure distribution $p(x)$ and strip semi-thickness $b(x)$ through the bite as the thickness of strip is varied. A set of six such solutions from (a) (inlet thickness, $h_0 = 2b_0 =$ 0.140 mm) to (f) ($h_0 = 2b_0 = 0.013$ mm) are presented in Fig. 1. Other parameters are held constant: roll radius R (89 mm), reduction r (50 per cent), coefficient of friction μ (0.03), plane strain yield stress Y_s (230 MPa), plane strain elastic modulus of the rolls E_R^* (230 GPa). Note the distortion of scales for strip semi-thickness b in Fig. 1. The ratio of vertical to horizontal magnification varies from 85 in case (a) to 910 in case (b).

In case (a) ($h_0 = 0.140$ mm) the deformation in the rolls is small and is adequately allowed for by the Hitchcock formula. Plastic reduction occurs throughout

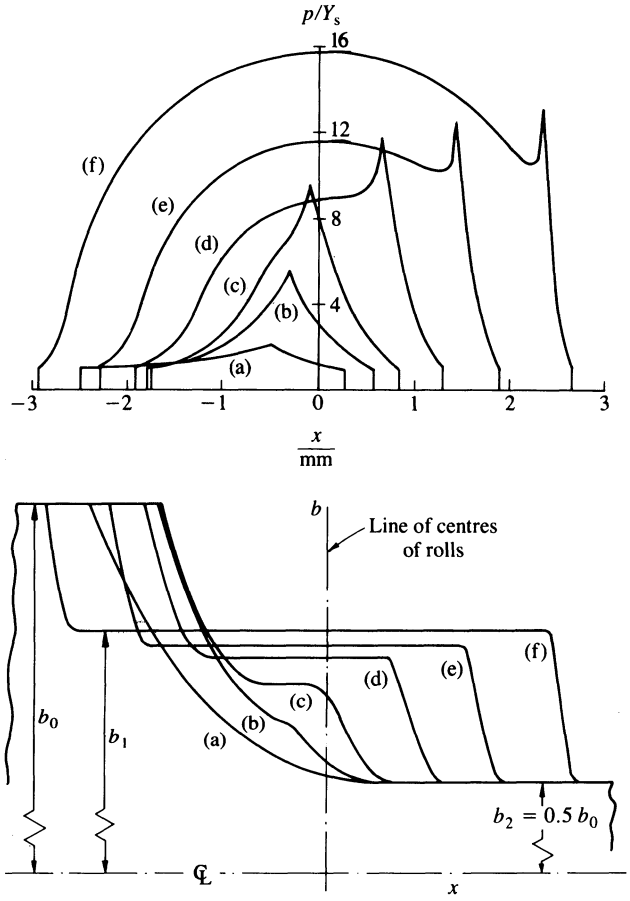

Fig. 1 Effect of strip thickness upon pressure distribution and deformed shape of strip. $R = 89$ mm, $\mu = 0.03$, $Y_s = 230$ MPa, $\sigma_0 = \sigma_2 = 0$, $E_R^* = 3$ $E_s^* = 230$ GPa, $r = 50\%$; (a) $h_0 = 2b_0 = 0.140$ mm, (b) $h_0 = 0.060$ mm, (c) $h_0 = 0.048$ mm, (d) $h_0 = 0.030$ mm, (e) $h_0 = 0.020$ mm, (f) $h_0 = 0.013$ mm

the bite: slip occurs everywhere, changing direction at the neutral section where the pressure peaks. The pressure distribution $p(x)$, shown in Fig. 1, case (a), and (as will be seen) the roll load and torque are given closely by the Bland and Ford theory (**3**).

In case (b) ($h_0 = 0.060$ mm) the increased sharp peak in pressure produces a departure from the circular deformed arc in the form of a noticeable indentation of the roll profile. This is the behaviour analysed by Jortner *et al.* (**9**) and confirmed by the present calculations. As in case (a), plastic reduction is continuous and slip occurs everywhere except at the neutral section. This regime of behaviour will be called 'regime I'.

The Jortner and Grimble theories (**9**) assume that slip takes place at all points. If this assumption were applied to case (c) ($h_0 = 0.048$ mm) it would be found that the pressure peak causes the rolls to deform locally to a concave shape. This behaviour is unacceptable since it implies an *increase* in thickness of the strip within the bite. The paradox is resolved by recognizing the existence of a *neutral zone* of finite length in which there is no slip between the strip and the rolls. The absence of slip has the effect of fully 'containing' any plastic reduction of the strip to an elastic order of magnitude. The thickness of the strip in such a no-slip zone is effectively uniform and the contact pressure adjusts to satisfy this condition.

With decreasing strip thickness in cases (d) ($h_0 = 0.030$ mm), (e) ($h_0 = 0.020$ mm) and (f) ($h_0 = 0.013$ mm) the length of the no-slip neutral zone increases and plastic reduction is confined to short zones at entry and exit. To flatten a segment of an elastic cylindrical roll requires the semi-elliptical pressure distribution of Hertz. This form of pressure distribution is evident in cases (e) and (f) which have extensive flat no-slip zones. A characteristic feature of the pressure distribution for thin strip is the sharp pressure peak which occurs just beyond the end of the neutral zone and which persists for overall reductions much less than 50 per cent. It is associated with the rather sharp re-entrant corner in the roll deformation at the onset of plastic reduction at exit and is discussed in Appendix 3.

In cases (c) and (d), where the pressure rises steadily through the no-slip zone, the stresses in the strip in that zone are at yield and the material is in a state of contained plastic flow. This regime of behaviour will be called 'regime II'. If the pressure falls in the no-slip zone, as it does after the line of centres in cases (e) and (f), elastic unloading of the strip can occur. This is 'regime III'. The details of this behaviour are discussed in Appendix 2.

It is apparent that the bite contains a number of separate zones, depending upon the regime of operation:

1. *Elastic zone at entry.* The strip is slipping backwards relative to the rolls. For practical values of reduction this zone is very small and can be neglected.
2. *Plastic reduction at entry.* The thickness is reduced from $2b_0$ to $2b_1$.
3. *No-slip neutral zone.* The strip thickness is approximately constant at $2b_1$. If the pressure gradient $\mathrm{d}p/\mathrm{d}x$ is positive throughout the neutral zone [for example Fig. 1, case (d)], the strip is in a state of contained plastic flow. A decreasing pressure [for example Fig. 1, cases (e) and (f)] can lead to elastic unloading.
4. *Plastic reduction at exit.* The thickness reduces from $2b_1$ to $2b_2$. A peak in pressure occurs where the slip direction reverses.
5. *Elastic zone at exit.* This is again small for practical reductions.

To proceed it is now necessary to establish the equations that have to be satisfied in these different zones.

3 GOVERNING EQUATIONS

3.1 Strip

An element of strip in the bite is shown in Fig. 2a. The strip enters with thickness $h_0 = 2b_0$ and is compressed in plane strain to a thickness $h(x) = 2b(x)$ at a position x from the line of centres of the rolls. The rolls exert a pressure $p(x)$ and a frictional traction $q(x)$ on the surface of the element. If $\bar{\sigma}_x(x)$ denotes the *average* longitudinal stress on the cross-section, and the gradient of the profile $\mathrm{d}b/\mathrm{d}x$ is small, equilibrium of the element gives

$$b(x)\frac{\mathrm{d}\bar{\sigma}_x}{\mathrm{d}x} + \{\bar{\sigma}_x(x) + p(x)\}\frac{\mathrm{d}b}{\mathrm{d}x} + q(x) = 0 \tag{1}$$

For strip which is thin compared with the length of the bite, during plastic deformation the Prandtl stress field [see reference (**10**)] is a good approximation:

$$\sigma_z(z) = -p \tag{2a}$$

$$\tau_{zx}(z) = \frac{qz}{b} \tag{2b}$$

$$(\sigma_x - \sigma_z)^2 + 4\tau_{zx}^2 = Y_s^2 \tag{2c}$$

which gives

$$\sigma_x(z) + p = Y_s\sqrt{\left\{1 - \left(\frac{2qz}{bY_s}\right)^2\right\}}$$

where z is the height above the centre-plane of the strip. Averaging through the thickness gives

$$\bar{\sigma}_x + p = Y_s I(m) \tag{3}$$

where

$$I(m) = \frac{\sin^{-1} m + m\sqrt{(1 - m^2)}}{2m}$$

and $m = 2q/Y_s$. The factor $I(m)$ reduces from 1.0 to $\pi/4$ as m increases from 0 to 1.0. Thus, provided the frictional traction q is appreciably less than the yield stress in shear ($Y_s/2$), the yield criterion (3) may be written

$$\bar{\sigma}_x(x) + p(x) \simeq Y_s \tag{3a}$$

This equation will be used in conjunction with equation (1) where the strip undergoes plastic reduction, and σ_x (without the overbar) will be used to denote the longitudinal stress averaged through the thickness.

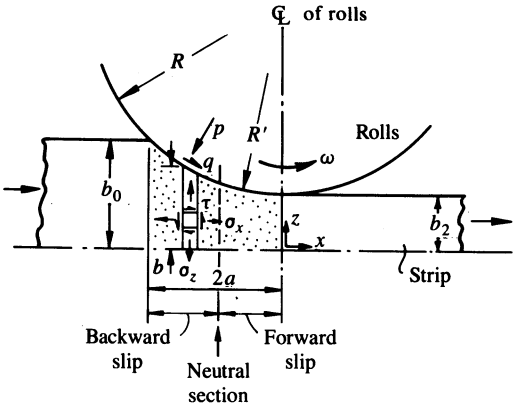

(a)

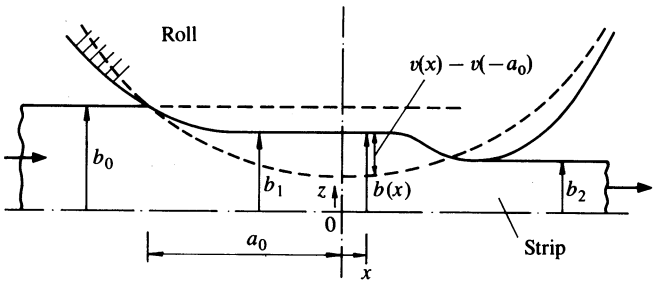

(b)

Fig. 2 Definition of stresses and nip geometry

Reduction in thickness of the strip due to *elastic* compression is neglected in comparison with the elastic compression of the rolls. Longitudinal elastic strain in the strip is important in its influence on slip. The total (elastic + plastic) longitudinal strain in the strip ε_s may be expressed as

$$\varepsilon_s = \varepsilon_s^e + \varepsilon_s^p = \frac{1}{E_s^*}\left\{\sigma_x(x) + \frac{\nu_s}{1-\nu_s}p(x)\right\} + \varepsilon_s^p \tag{4}$$

where ε_s^p is the longitudinal plastic strain in the strip, ε_s^e is the longitudinal elastic strain in the strip and ν_s and E_s^* are the Poisson ratio and the plane strain Young modulus for the strip.

3.2 Rolls

Provided the contact length is small compared with the radius R of the rolls, the undeformed profile of the upper rolls $z(x)$ may be approximated by

$$z(x) = b_0 - (a_0^2 - x^2)/2R \tag{5}$$

where $-a_0$ is the coordinate of the point of entry to the nip. This point is taken as a datum for normal displacements. The semi-thickness $b(x)$ of the strip at any point x in the bite is then related to the elastic compression of the roll $v(x)$ at that point by (see Fig. 2b)

$$b(x) = b_0 - \frac{a_0^2 - x^2}{2R} + v(x) - v(-a_0) \tag{6}$$

The effect of the frictional traction $q(x)$ on normal displacement is negligible [reference (**11**), p. 20], whereupon

$$v(x) - v(-a_0) = \frac{2}{\pi E_R^*}\int_{-a_0}^{a_2} p(x') \ln\left|\frac{a_0 + x'}{x - x'}\right| dx' \tag{7}$$

where a_2 is the exit point. Combining equations (6) and (7) gives

$$b(x) = b_0 - \frac{a_0^2 - x^2}{2R} + \frac{2}{\pi E_R^*}\int_{-a_0}^{a_2} p(x') \ln\left|\frac{a_0 + x'}{x - x'}\right| dx' \tag{8}$$

3.3 Interface

In a region of slip between the strip and the rolls, the frictional traction $q(x)$ is related to the normal pressure $p(x)$ by the Coulomb law:

$$q(x) = \alpha\mu p(x) \tag{9a}$$

where $\alpha = +1$ when the strip is moving slower than the rolls and $\alpha = -1$ when it is moving faster.

In a region where there is no-slip

$$|q(x)| \leqslant \mu p(x) \tag{9b}$$

and the strip and the surface of the rolls move with the same velocity. This condition demands that the difference in longitudinal strain between the rolls and the strip is constant and given by [see reference (**11**), p. 242]

$$\varepsilon_R(x) - \varepsilon_s(x) = \frac{V_s - V_R}{V_R} \equiv \text{constant } \xi \tag{10}$$

where V_R is the peripheral speed of the undeformed roll, V_s is the entry speed of the strip and the constant ξ is the 'creep ratio'. The longitudinal strain in the strip ε_s is given by equation (4) and that in the surface of the rolls is given by [see reference (**11**), p. 20]

$$\varepsilon_R(x) = \frac{\partial u_x}{\partial x} = -\frac{1-2\nu_R}{1-\nu_R}\frac{1}{E_R^*}p(x) - \frac{2}{\pi E_R^*}\int_{-a_0}^{a_2}\frac{q(x')}{x - x'}dx' \tag{11}$$

Substituting expressions for $\varepsilon_s(x)$ and $\varepsilon_R(x)$ from equations (4) and (11) into equation (10) gives the condition of no-slip:

$$\sigma_x(x) + \left(\frac{\nu_s}{1-\nu_s} + \frac{1-2\nu_R}{1-\nu_R}\frac{E_s^*}{E_R^*}\right)p(x) + \frac{2}{\pi}\frac{E_s^*}{E_R^*}J(x) + E_s^*\varepsilon_s^p = -E_s^*\xi \tag{12}$$

where

$$J(x) = \int_{-a_0}^{a_2}\frac{q(x')}{x - x'}dx'$$

3.4 Assembly of equations in each zone

The equations can now be assembled which have to be satisfied in the different zones in order to solve for the pressure distribution $p(x)$ and the deformed shape $b(x)$ throughout the bite.

3.4.1 Elastic slip (elastic zones at entry and exit)

Since transverse elastic compression of the strip is neglected $db/dx = 0$, so that equation (1) reduces to

$$b\frac{d\sigma_x}{dx} + \alpha\mu p(x) = 0 \tag{13}$$

where $b = b_0$ at entry and b_2 at exit.

3.4.2 Elastic no-slip (neutral zone)

Here the plastic strain in the strip is constant: $\varepsilon_s^p = (b_0 - b_1)/b_0$, so that equation (12) becomes

$$\sigma_x(x) + \left(\frac{\nu_s}{1-\nu_s} + \frac{1-2\nu_R}{1-\nu_R}\frac{E_s^*}{E_R^*}\right)p(x) + \frac{2}{\pi}\frac{E_s^*}{E_R^*}J(x) = \text{constant (C)} \tag{14}$$

Note that, for practical values of μ, $q(x)$ is always much smaller than $p(x)$ and, for aluminium strip, $E_s^* \simeq \frac{1}{3}E_R^*$, so that the term in $J(x)$ in equation (14) is relatively small. Thus

$$\sigma_x(x) + 0.62\ p(x) \simeq C \tag{14a}$$

3.4.3 Plastic reduction

Since slip must accompany plastic reduction except at a neutral point and the yield condition (3a) applies, equation (1) becomes

$$-b(x)\frac{dp}{dx} + Y_s\frac{db}{dx} + \alpha\mu p = 0 \tag{15}$$

3.4.4 Plastic no-slip (contained plastic)

If the condition for elastic no-slip, given by equation (14), cannot be satisfied without violating the yield condition (3a), then some plastic deformation must occur according to equation (12). However, the elastic strains in the rolls, given by equation (11), are small, which demands that any plastic strain in the strip ε_s^p must be *constant to an elastic order of magnitude* to satisfy the no-slip condition equation (14). Thus variations in thickness of the strip due to contained plastic deformation may be ignored compared with the elastic compression of the rolls. For the purpose of calculating the roll pressure $p(x)$, it may be assumed that $b(x) =$ constant $= b_1$ in the neutral zone. Equation (1) then becomes

$$b_1\frac{d\sigma_x}{dx} + q(x) = -b_1\frac{dp}{dx} + q(x) = 0 \tag{16}$$

The roll deformation equation (8) applies throughout the bite. It must be solved simultaneously with equation (15) in the plastic reduction zones. In the elastic zone at entry, the neutral zone and the elastic zone at exit the thickness of the strip is constant at b_0, b_1 and b_2 respectively. Given the entry position a_0, initial strip thickness b_0, entry and exit tensions σ_0 and σ_2, we determine the pressure distribution $p(x)$ and the deformation $b(x)$ throughout the bite. The subdivision of the neutral zone into elastic and contained plastic zones, leading to the determination of the stress in the strip $\sigma_x(x)$ and the frictional traction $q(x)$ throughout the bite, is found by a subsequent calculation using equations (14) and (16).

4 NUMERICAL IMPLEMENTATION

To solve the integral and differential equations (8) and (11) for the deformation of the rolls, the pressure $p(x)$ and frictional traction $q(x)$ are approximated by piecewise linear distributions, as shown in Fig. 10. The contact arc is divided into a total of N (typically 100) overlapping triangular elements. The $N + 1$ points at the ends of the elements, equally spaced a distance c apart, are termed nodes. The unknowns of the problem are the values of p_j, q_j and b_j at the nodes. The displacement v_i and the displacement gradient $(\partial u/\partial x)_i$ are obtained by summing the contributions from each element of traction over the whole contact arc. Thus

$$v_i = C_{ij}q_j + D_{ij}p_j \tag{17}$$

$$\left(\frac{\partial u}{\partial x}\right)_i = C'_{ij}q_j + D'_{ij}p_j \tag{18}$$

where a repeated suffix denotes summation over the $N + 1$ nodes. As mentioned earlier, the problem is greatly simplified by neglecting the effect of frictional traction q upon the normal displacement v, that is by putting $C_{ij} = 0$ in equation (17). This has the effect of decoupling equation (8) for the pressure from equation (11) for the frictional traction. The influence coefficients D_{ij}, C'_{ij} and D'_{ij} for triangular elements are easily obtained in closed form [reference (**11**), pp. 27, 148]. Expressions are given in Appendix 1. In discrete form equation (8) for the roll deformations becomes

$$b_i = b_0 - \frac{a_0^2 - x_i^2}{2R} + v_i - v(-a_0) \tag{19}$$

where, by equation (17), $v_i = D_{ij}p_j$ and $v(-a_0) = D_{0j}p_j$.

In a plastic reduction zone the equilibrium equation (15) for the strip can be integrated over an element from x_{i-1} to x_i, assuming a piecewise linear variation of both pressure $p(x)$ and the inverse of the thickness $1/b(x)$, to obtain

$$p_i = \frac{Y_s \ln\left(\dfrac{b_i}{b_{i-1}}\right) + p_{i-1}\left\{1 - \alpha\mu c\left(\dfrac{1}{3b_{i-1}} + \dfrac{1}{6b_i}\right)\right\}}{1 + \alpha\mu c\left(\dfrac{1}{3b_{i-1}} + \dfrac{1}{6b_i}\right)} \tag{20}$$

Within the central neutral zone $b_i =$ constant (b_1). Numerical experimentation has shown that for practical reductions ($r > 10$ per cent) the *elastic* zones at entry and exit are very short and can be neglected. Thus at entry $b(-a_0) = b_0$ and $p(-a_0) = Y_s - \sigma_0$; at exit $(db/dx)_2 = 0$ and $p(x_2) = Y_s - \sigma_2$.

To obtain a solution, values of a_0, b_0, σ_0 and σ_2 are selected. The strategy consists of iterating the pressure distribution. At each stage the deformed thickness of the strip b_i is given in terms of the current pressure by equation (19); equation (20) is then used to update the pressure. To obtain a fully converged solution, however, it is also necessary to locate the boundaries of the different zones discussed in Section 2. Details of the procedures

to obtain complete solutions in the three different regimes defined in Section 2 are outlined in Appendix 2.

A further feature of the regime III [cases (e) and (f) in Fig. 1] calls for comment: the sharp pressure peak close to the end of the neutral zone. This feature gave rise to numerical difficulties in the form of unbounded pressures. Accordingly an asymptotic solution in closed form in the vicinity of the peak was sought (**12**). It is based on concepts from fracture mechanics and is discussed in Appendix 3. Two conclusions follow from this analysis: (*i*) for the pressure to be bounded and continuous through the peak there should be no discontinuity in surface gradient db/dx through the peak and (*ii*) a small region of plastic reduction must exist to the left of the peak, in which the strip slips backwards relative to the rolls. The peaks in regime III [cases (e) and (f) in Fig. 1] are located at neutral sections in the same way as the peaks in cases (a), (b), (c) and (d). The fact of no-slip at the peak determines the value of the creep ratio ξ in equation (12). With this value of ξ, the condition of no-slip is satisfied in the contained plastic zone by plastic flow ε_s^p of appropriate magnitude.

5 RESULTS

5.1 Dimensional analysis

Within the idealization of the problem outlined above the dependent variables are: strip thickness $b(x)$ and roll pressure $p(x)$ at a location x relative to the centre-line of the rolls, and the roll load W and torque Q per unit length of the rolls. The independent variables are: front and back tensions σ_0 and σ_2, radius R and plane strain modulus E_R^* of the rolls, inlet thickness $2b_0$ and plane strain yield stress Y_s of the strip, and the coefficient of friction μ. Appropriate non-dimensional variables are sought.

By writing

$$X = \left(\frac{xE_R^*}{RY_s}\right); \qquad B = \left(\frac{bE_R^{*2}}{RY_s^2}\right); \qquad P = \frac{p}{Y_s};$$
$$U = \frac{\mu E_R^*}{Y_s}; \qquad \Sigma_0 = \frac{\sigma_0}{Y_s}; \qquad \Sigma_2 = \frac{\sigma_2}{Y_s} \tag{21}$$

the roll deformation equation (8) can be written as

$$B(X) = B_0 - \tfrac{1}{2}(X_0^2 - X^2) + \frac{2}{\pi}\int_{X_0}^{X_2} P(X') \ln\left|\frac{X_0 - X'}{X - X'}\right| dX' \tag{22}$$

and equation (15) for plastic deformation of the strip as

$$-B(X)\frac{dP}{dX} + \frac{dB}{dX} + \alpha U P(X) = 0 \tag{23}$$

Given σ_0, B_0 and U, and an arbitrary choice of inlet position X_0 ($= -a_0 E_R^*/RY_s$), the exit boundary conditions determine the location X_2 ($= a_2 E_R^*/RY_s$) of the exit.

Thus

$$P(X), B(X) = f[B_0, X_0, U, \Sigma_0, \Sigma_2] \tag{24}$$

The roll load per unit length is given by

$$W = \int_{-a_0}^{a_2} p(x)\, dx$$

or

$$\bar{W} \equiv \frac{WE_R^*}{RY_s^2} = \int_{X_0}^{X_2} P(X)\, dX \tag{25}$$

and the roll torque per unit length by

$$Q = \int_{-a_0}^{a_2} p(x)x\, dx + (\sigma_0 b_0 - \sigma_2 b_2)R$$

or

$$\bar{Q} \equiv \frac{QE_R^{*2}}{R^2 Y_s^3} = \int_{X_0}^{X_2} P(X)X\, dX + B_0\Sigma_0 - B_2\Sigma_2 \tag{26}$$

In particular equation (22) yields the exit thickness $B_2 (= b_2 E_R^{*2}/RY_s^2)$ and hence the reduction

$$r = \frac{b_0 - b_2}{b_0} = \frac{B_0 - B_2}{B_0} \tag{27}$$

This enables X_0 to be eliminated so that

$$\bar{W}, \bar{Q} = f[B_0, U, r, \Sigma_0, \Sigma_2] \tag{28}$$

The roll load and torque are governed by five independent non-dimensional parameters representing the effects of thickness $B_0 = (b_0 E_R^{*2}/RY_s^2)$, reduction r, friction $U = (\mu E_R^*/Y_s)$, and front and back tensions $\Sigma_0 = \sigma_0/Y_s$ and $\Sigma_2 = \sigma_2/Y_s$. These variables will be used in the presentation of results.

5.2 Distributions of $p(x)$, $b(x)$, $\sigma_x(x)$ and $q(x)$

A selection of distributions of pressure and strip thickness through the nip with varying initial thickness is presented in Fig. 1 and has been discussed qualitatively in Section 2. Three regimes of behaviour were identified: I (thicker strips) plastic reduction is continuous; II (intermediate thickness) plastic reduction takes place at entry and exit separated by a neutral (no-slip) zone of contained plastic deformation; III (thinner strips) the pressure reaches a maximum and then falls, leading to elastic unloading of the strip. Complete solutions for pressure $p(x)$, thickness $b(x)$, strip tension $\sigma_x(x)$ and frictional tractions $q(x)$ representative of the three regimes are presented in Fig. 3.

The pressure distribution in regime I (Fig. 3a) displays the familiar 'friction hill', with a peak at the neutral section where the slip and hence the friction change sign. As explained in Appendix 3, this peak, coinciding with a reversal of slip and friction, persists in regimes II (Fig. 3b) and III (Fig. 3c) and is located near the downstream end of the neutral zone. It follows from equation (15) that reducing the strip thickness increases the height of the friction hill and hence leads to increasing contact pressures and roll deformation.

The results presented in this paper are all for zero front and back tensions. In these circumstances the plastic reductions in entry and exit zones are of comparable magnitude. However, it is apparent from Fig. 1 that the reduction at entry as a fraction of the total reduction decreases with decreasing strip thickness.

Apart from the small elastic zones at entry and exit which have been neglected, the different zones are shown in Fig. 3. The conditions which fix the positions

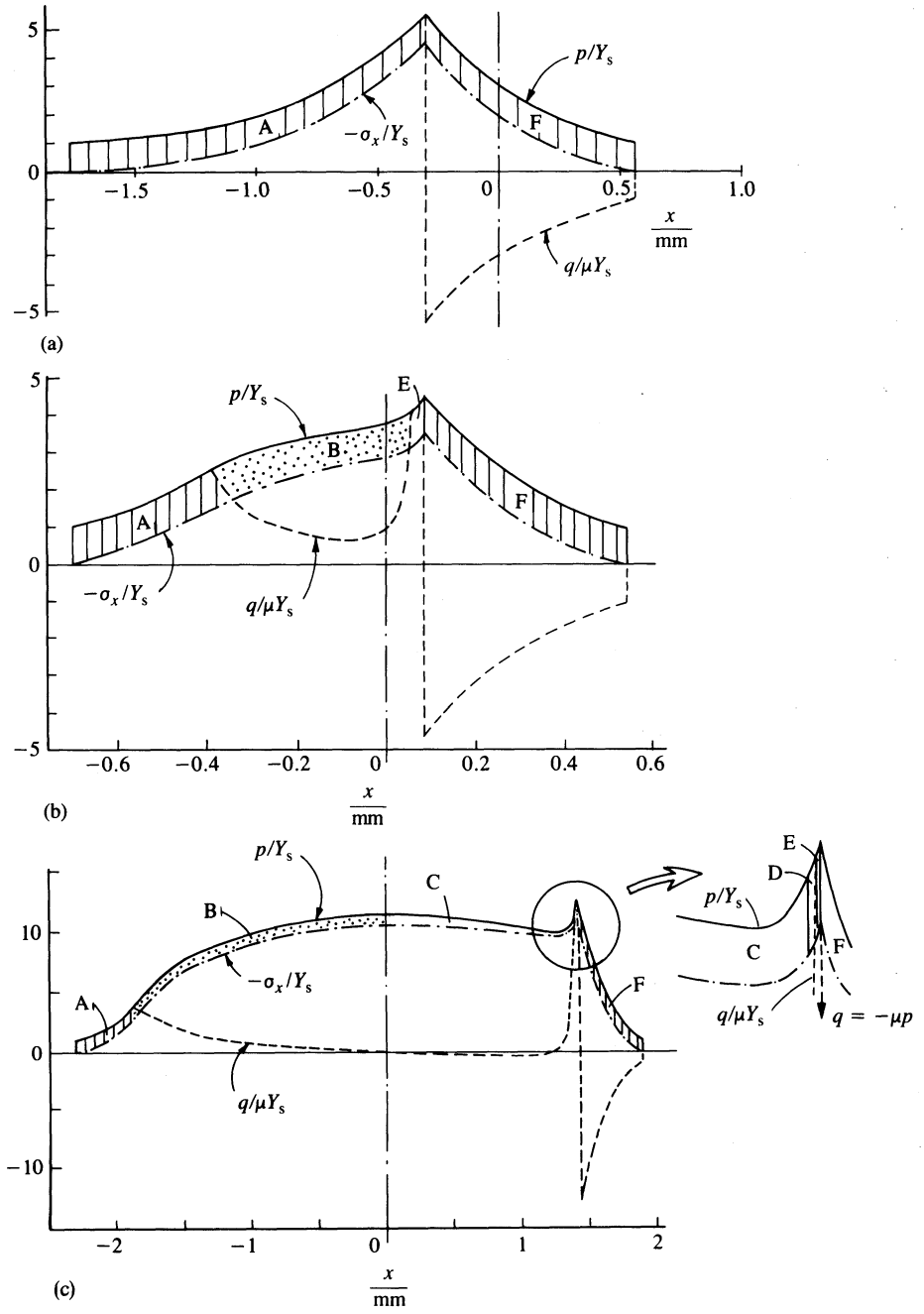

Fig. 3 Regimes of strip behaviour. Note that zones A and E experience plastic reduction with backward slip. Zones B and D experience contained plastic deformation with no slip. Zone C experiences elastic deformation with no slip and zone F experiences plastic reduction with forward slip. In all cases $R = 89$ mm, $\mu = 0.03$, $Y_s = 230$ MPa and $E_R^* = 230$ GPa
(a) Regime I ($h_0 = 2b_0 = 0.060$ mm, $r = 50\%$)
(b) Regime II ($h_0 = 2b_0 = 0.020$ mm, $r = 10\%$)
(c) Regime III ($h_0 = 2b_0 = 0.020$ mm, $r = 50\%$)

of the boundaries of the different zones are discussed in Appendix 2.

5.3 Roll load and torque

Once the pressure distributions have been found the roll load and torque can be computed from equations (25) and (26). The calculated values of non-dimensional roll load $\bar{W}$ are plotted as a function of non-dimensional strip thickness B_0 and reduction r in Fig. 4, for $U = 30$. The corresponding plot for roll torque $\bar{Q}$ is given in Fig. 5. Note that $\bar{W}$ increases with increasing reduction. For a given reduction $\bar{W}$ increases with decreasing strip thickness in regimes II and III. However, no limiting gauge is predicted. There is a dramatic switch in the $\bar{W}$–B_0 response as the strip thickness is reduced from the Jortner regime I to regimes II and III. At large strip thicknesses, in regime I, the load response merges into the Bland and Ford (3) solution. In regimes II and III the $\bar{W}$–B_0 response is almost linear on log–log axes: contours of finite reduction are roughly parallel to the

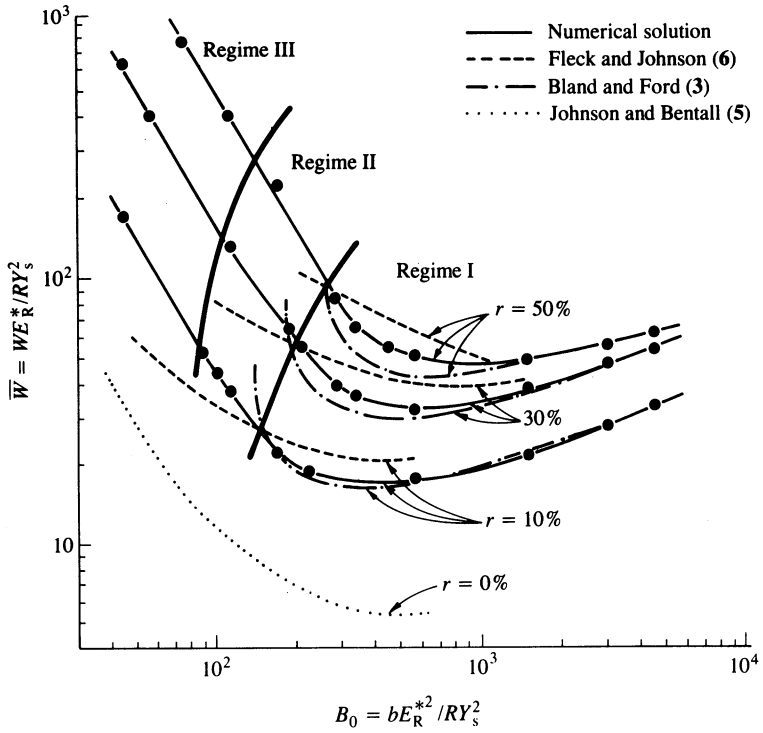

Fig. 4 Effect of entry strip thickness $B_0 = bE_R^{*2}/RY_s^2$ and reduction r upon roll load $\bar{W} = WE_R^*/RY_s^2$; $U = \mu E_R^*/Y_s = 30$

onset of reduction solution given by Johnson and Bentall (5).

Now consider the torque response in Fig. 5. $\bar{Q}$ increases with increasing reduction r as expected. At large strip thicknesses, in regime I, the contact region lies to the left of the centre-line of the rolls, as shown in Fig. 2; the pressure distribution acts through a large lever arm and the torque is high. As the strip thickness is reduced the centre of pressure of the nip moves towards the centre-line of the rolls and $\bar{Q}$ decreases. In the limiting case of zero reduction (5) $p(x)$ is symmetric about the centre-line of the rolls and $\bar{Q}$ is zero.

Results for $\bar{W}$ and $\bar{Q}$ as a function of B_0, U and r were each successfully collapsed on to a single 'master curve', by a multi-variable regression analysis. The combinations of non-dimensional groups to achieve this are $\{\bar{W}U^{-0.70}r^{-0.70}\}$, $\{\bar{Q}U^{-1.34}r^{-1.62}\}$ and $\{B_0\,U^{-1.24}r^{-0.50}\}$, as shown in Fig. 6. Data are shown for a wide range of values for B_0, U and r. The boundaries between regimes I, II and III are also shown. For

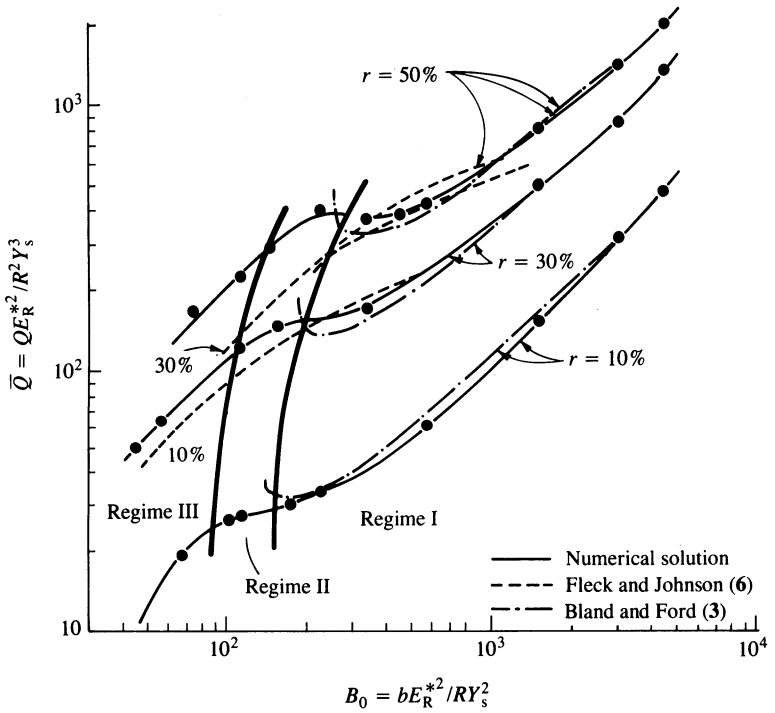

Fig. 5 Effect of entry strip thickness $B_0 = bE_R^{*2}/RY_s^2$ and reduction r upon roll torque $\bar{Q} = QE_R^{*2}/R^2Y_s^3$; $U = \mu E_R^*/Y_s = 30$

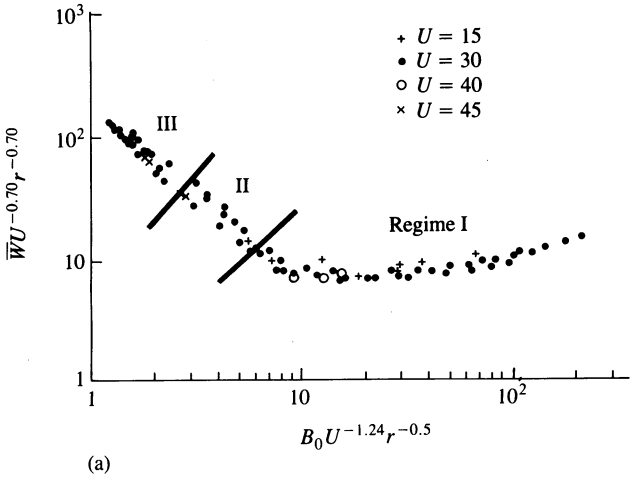

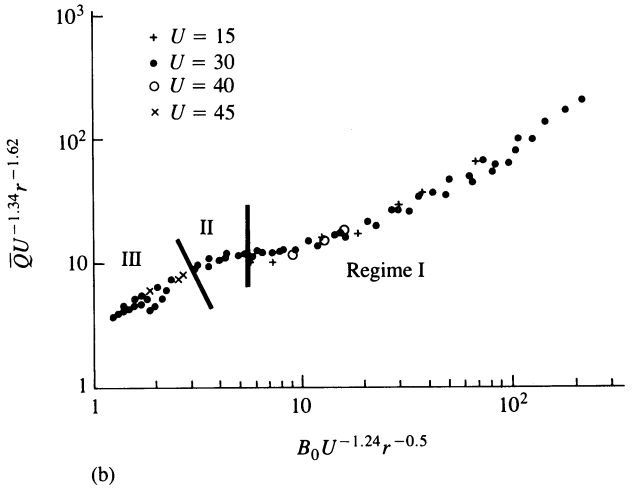

Fig. 6 Master curves for (a) roll load and (b) roll torque, for $10\% \leqslant r \leqslant 50\%$, $15 \leqslant U \leqslant 45$ and $2 \leqslant \bar{H} \leqslant 300$

example the boundary between regions I and II occurs at

$$B_0\,U^{-1.24}r^{-0.50} \simeq 6$$

that is at a critical inlet gauge h_{0c} given by

$$\frac{h_{0c}}{R} = \frac{2b_{0c}}{R} \simeq 12\, r^{0.5}\mu^{1.24}\left(\frac{Y_s}{E_R^*}\right)^{0.76} \tag{29}$$

It is not clear why this particular combination of non-dimensional groups is able to correlate the results, but some insight is gained by the observation that the independent variable $\{B_0\,U^{-1.24}r^{-0.50}\}$ correlates with the parameter $\{2b_0/\mu l\}$ as shown in Fig. 7. Here, $2b_0$ is the inlet strip thickness and l is the length of the contact region so that $2b_0/l$ is the aspect ratio of the nip. The parameter $2b_0/\mu l$ is also the dominant non-dimensional group in the Bland and Ford regime, as discussed by Johnson (**11**).

5.4 Comparison with rolling mill data

Direct comparison of the theoretical results with measured data for a rolling mill is difficult because of the lack of knowledge of a value for the Coulomb friction coefficient μ. The approach adopted is to equate the theoretical and experimental values of the roll load in order to deduce a value for μ, and then use the theory to predict the torque.

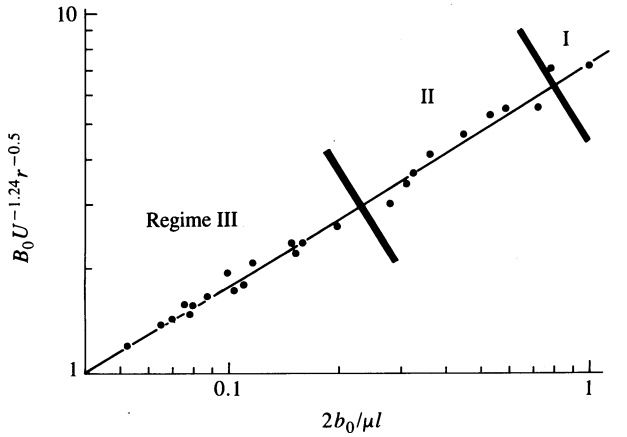

Fig. 7 Correlation of aspect ratio of nip $2b_0/\mu l$ with the combination of non-dimensional groups $B_0\,U^{-1.24}r^{-0.5}$, for $10\% < r < 50\%$, $15 \leqslant U \leqslant 45$ and $2 \leqslant \bar{H} \leqslant 300$

Calculations were carried out as described above for values for strip thickness, and front and back tension in accordance with mill data provided by Davy–McKee (Poole) Limited. Non-dimensional load $\bar{W}$ and torque $\bar{Q}$ are plotted against the friction parameter U in Fig. 8. The measured load $\bar{W} = 58$ gives $\mu = 0.026$. Using this value of μ the predicted torque is $\bar{Q} = 370$; the measured torque is $\bar{Q} = 480$. The torque was measured by strain gauges in the drive shafts and is accurate to within 10 per cent. A discrepancy between the prediction and the measurement remains, which is most likely to be a consequence of the simple Coulomb model of friction.

5.5 Comparison with the theory of Fleck and Johnson

The predicted roll loads and torques are shown in Figs 4 and 5 for the current theory, the Fleck–Johnson theory (**6**) and the Bland and Ford (**3**) theory. Note that the three models converge at large strip thicknesses ($B_0 > 10^3$) as expected. The Fleck and Johnson model diverges from the current theory as strip thickness is reduced. At all reductions 10 per cent $\leqslant r \leqslant$ 50 per cent,

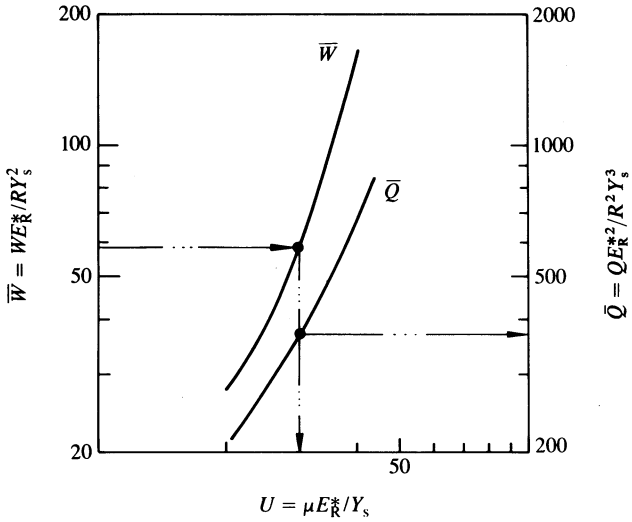

Fig. 8 Comparison of model with mill data. $b_0 = 0.0365$ mm, $Y_s = 230$ MPa, $r = 57\%$, $\sigma_0 = 0.107\,Y_s$, $\sigma_2 = 0.132\,Y_s$, 1100 aluminium alloy on third pass

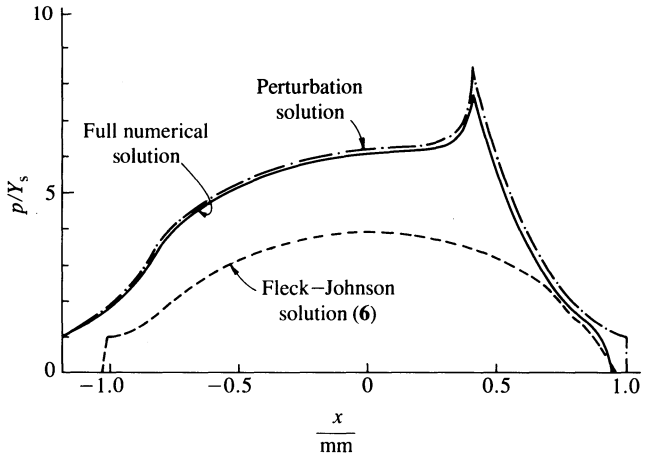

Fig. 9 Comparison of full numerical solution, perturbation solution and Fleck and Johnson (**6**) solution, for the case $R = 89$ mm, $b_0 = 0.01$ mm, $r = 25\%$, $Y_s = 230$ MPa, $E_R^* = 230$ GPa, $E_s^* = 80$ GPa, $\mu = 0.03$, $\sigma_0 = \sigma_2 = 0$, $B_0 = 112$. The full numerical solution gives $\bar{W} = 118$, the perturbation solution gives $\bar{W} = 120$ and the Fleck and Johnson (**6**) solution gives $\bar{W} = 62$

the Fleck and Johnson model underpredicts rolling load by up to a factor of 2. The two models agree in their prediction of torque to within a factor of 2 for 30 per cent $\leqslant r \leqslant 50$ per cent. At $r = 10$ per cent, the Fleck and Johnson model predicts torques which are an order of magnitude below those of the current theory. A comparison of pressure distributions is shown in Fig. 9 for a particular case where $r = 25$ per cent.

6 CONCLUDING DISCUSSION

In treating the rolls as elastic half-spaces the theory presented in this paper is considerably more rigorous than the earlier theory of Fleck and Johnson (**6**) which assumed that the perturbation in the deformed shape of the rolls from the Hertzian profile is that of an elastic foundation. In contrast with earlier work, both theories predict that with thin gauges plastic reduction zones at entry and exit are separated by a neutral zone in which there is no slip between the strip and the rolls and hence no significant reduction in thickness. The more rigorous treatment of roll deformation reveals a sharp 'friction hill' just beyond the exit to the neutral zone, which was absent in the earlier analysis. These differences lead to a difference in the relative amount of plastic reduction at entry and exit and to a significant quantitative difference in the predicted roll loads and torques. The present theory is expected to be more reliable in all these respects.

The principal idealizations in the theory are:

(a) no strain hardening
(b) homogeneous deformation
(c) constant coefficient of Coulomb friction.

In the final stands of an aluminium foil mill the rate of strain hardening is small, typically 4 per cent through the penultimate stand. Some allowance for strain hardening could easily be made by ascribing different values of Y_s to the reduction zones at entry and exit.

In assuming homogeneous plastic deformation equation (3a) has been taken as the yield condition, that is $I(m)$ in equation (3) has been assumed to be unity. Now $I(m)$ exceeds 0.9 provided $m(= 2\mu p/Y_s) < 0.7$. Data provided by Davy–McKee from tests on a rolling mill suggest a value for μ of 0.03, so that this condition is satisfied (just) for all the plastic reduction zones shown in Fig. 1.

The most contentious idealization in this analysis lies in the use of a constant coefficient of friction. The evidence from foil mill practice that the reduction is sensitive to speed strongly suggests a hydrodynamic component in the friction. However, the calculated film thickness is of the order of 0.1 μm, which is comparable with the roughness of the strip, so that operation is in the so-called 'mixed lubrication' regime. There seems to be no point in refining the rolling model until more is known about the nature of friction in the roll bite. Some steps in this direction have been taken recently by Sutcliffe (**13, 14**).

ACKNOWLEDGEMENTS

The project has been sponsored jointly by Davy–McKee (Poole) Limited and Alcan International (Banbury Laboratories). The authors would also like to acknowledge the valuable technical input to the project by Dr T. A. Gore and Dr K. Waterson representing those companies respectively. The authors are also grateful for several discussions with Dr J. A. Greenwood and Dr M. P. F. Sutcliffe.

REFERENCES

1 **von Karmann, T.** Beitrag zür theorie des Walzvorganges. *Z. angeur. Math. Mech.*, 1925, **5**, 139.
2 **Orowan, E.** Graphical calculation of roll pressure with the assumptions of homogeneous compression and slipping friction. *Proc. Instn Mech. Engrs*, 1943, **150**, 141.
3 **Bland, D. R.** and **Ford, H.** The calculation of roll force and torque in cold strip rolling with tensions. *Proc. Instn Mech. Engrs*, 1948, **159**, 144.
4 **Hitchcock, J. H.** Roll neck bearings. Report of ASME Research Committee, 1935.
5 **Johnson, K. L.** and **Bentall, R. H.** The onset of yield in the cold rolling of thin strip. *J. Mech. Phys. Solids*, 1969, **17**, 253.
6 **Fleck, N. A.** and **Johnson, K. L.** Towards a new theory of cold rolling thin foil. *Int. J. Mech. Sci.*, 1987, **29**(7), 507–524.
7 **Grimble, M. J.** Solution of the nonlinear functional equations representing the roll gap relationships in a cold mill. *J. Optimization Theor. Applic.*, 1978, **26**(3), 427.
8 **Grimble, M. J., Fuller, M. A.** and **Bryant, G. F.** A non-circular arc roll force model for cold rolling. *Int. J. Num. Meth. Engng*, 1978, **12**, 643.
9 **Jortner, D., Osterle, J. F.** and **Zorowski, C. F.** An analysis of cold strip rolling. *Int. J. Mech. Sci.*, 1960, **2**, 179–194.
10 **Hill, R.** *The mathematical theory of plasticity*, 1950 (Oxford University Press, Oxford).
11 **Johnson, K. L.** *Contact mechanics*, 1985 (Cambridge University Press, Cambridge).
12 **Greenwood, J. A., Fleck, N. A.** and **Johnson, K. L.** *Modified Hertzian contacts* (to be published).
13 **Sutcliffe, M. P. F.** Experimental measurements of lubricant film thickness in cold strip rolling. *Proc. Instn Mech. Engrs*, Part B, 1990, **204**(B4), 263–273.
14 **Sutcliffe, M. P. F.** and **Johnson, K. L.** Lubrication in cold strip rolling in the 'mixed' regime. *Proc. Instn Mech. Engrs*, Part B, 1990, **204**(B4), 249–261.
15 **Barenblatt, G. I.** The mathematical theory of equilibrium cracks in brittle fracture. In *Advances in applied mechanics*, Vol. 7, 1962, pp. 59–129 (Academic Press, London).
16 **Schapery, R. A.** A theory of crack initiation and growth in viscoelastic media: I. Theoretical development. *Int. J. Fracture*, 1975, **11**(1), 141–159.

APPENDIX 1

Influence coefficients for a piecewise linear traction

A piecewise linear distribution of traction can be regarded as the superposition of overlapping triangular elements each of base $2c$ as shown in Fig. 10. The influence coefficient for the deflexion at $x = ic$ due to a pressure element centred at $x = jc$ is required. It follows from the expressions given in reference (**11**), p. 27, that the influence coefficients defined in equations (17) and (18) may be written

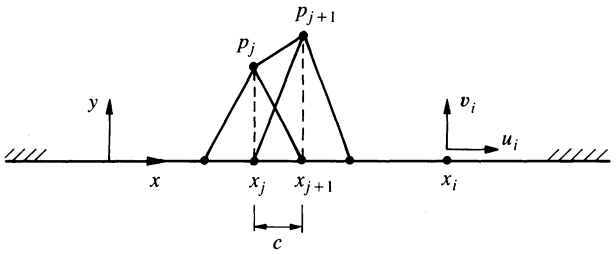

Fig. 10 Fundamental elasticity problem for the rolls

$$D_{ij} = \frac{c}{2\pi E_R^*}\{(k+1)^2 \ln(k+1)^2 + (k-1)^2 \ln(k-1)^2 - 2k^2 \ln k^2\} + \text{constant} \quad (30)$$

$$C'_{ij} = -\frac{1}{\pi E_R^*}\left\{(k+1)\ln\left(\frac{k+1}{k}\right)^2 + (k-1)\ln\left(\frac{k-1}{k}\right)^2\right\} \quad (31)$$

$$D'_{ij} = -\frac{1-2\nu_R}{(1-\nu_R)E_R^*}, \quad j = i$$
$$= 0, \quad j \neq i \quad (32)$$

where $k = i - j$.

APPENDIX 2

Solution procedure

The numerical implementation of the theory has been discussed in general terms in Section 4. To effect a solution it is first necessary, tentatively at least, to identify the regime of behaviour. Details of the procedure appropriate to each regime are given below.

Regime I

This is the Jortner regime in which plastic reduction and slip occurs throughout the nip [Fig. 3a; cases (a) and (b) in Fig. 1]. There are only two zones, A and F, of backward and forward slip. The boundary x_{AF} and the exit location x_2 are chosen arbitrarily. After converged distributions of pressure $p(x)$ and strip thickness $b(x)$ are obtained using equations (19) and (20), the positions of the boundaries x_{AF} and x_2 are moved by a Newton–Raphson procedure until the exit conditions $\sigma_x = \sigma_2$ and $db/dx = 0$ are satisfied at $x = x_2$. The value of reduction r associated with the chosen values of a_0 and b_0 follows from the exit thickness b_2.

When a converged solution for pressure is obtained the longitudinal stress in the strip and the frictional traction at the nodes are given by

$$(\sigma_x)_i = Y_s - p_i \quad (33)$$

and

$$q_i = \alpha\mu p_i \quad (34)$$

For a solution to exist in regime I, $db/dx \leqslant 0$ throughout the nip.

Regime II

For strips thinner than in regime I, a central no-slip zone of contained plastic deformation exists for the strip. This is shown in Fig. 3b and is exemplified by cases (c) and (d) of Fig. 1. In this regime the pressure increases monotonically from entry to the pressure spike.

The bite is split into four zones as shown in Fig. 3b: (A) plastic reduction with backward slip; (B) contained plastic deformation with no slip; (E) plastic reduction with backward slip; (F) plastic reduction with forward slip.

The solution procedure is to iterate the pressure distribution within the plastic reduction zones in a similar manner to that for regime I. We fix a_0 and b_0, guess initial values for the boundaries x_{AB}, x_{BE}, x_{EF} and a_2, and assume an initial pressure distribution in the plastic reduction zones A, E and F. Since the strip thickness is constant in the contained plastic zone B, equations (6) and (17) give

$$(D_{ij} - D_{(i-1)j})p_j = \frac{x_{i-1}^2 - x_i^2}{2R} \quad (35)$$

where j ranges over all nodes and i refers to nodes in the contained plastic zone. Equation (35) is used to deduce the pressure in the contained plastic zone from the assumed pressure distribution in the plastic reduction zones A, E and F. The strip thickness is then calculated from equation (19), where $v_i = D_{ij}p_j$. The pressure profile is updated in zones A, E and F by integrating the equilibrium equation, and in zone B by equation (35), until a converged solution for $p(x)$ and $b(x)$ is obtained. The boundaries x_{AB}, x_{BE}, x_{EF} and a_2 are moved in order to satisfy the four conditions:

1. Plastic reduction stops and hence $db/dx = 0$ at x_{AB}. This is equivalent to the statement dp/dx is continuous at x_{AB}.
2. Slip occurs at x_{BE} ($q = \mu p$). The shear stress $q(x)$ is calculated at nodes in the contained plastic zone by equation (16) in finite difference form:

$$b_1(p_{i+1} - p_{i-1}) - q_i(x_{i+1} - x_{i+1}) = 0 \quad \text{no sum on } i \quad (36)$$

3. $p = Y_s - \sigma_2$ at $x = a_2$.
4. Plastic reduction stops and hence $db/dx = 0$ at $x = a_2$.

Boundaries x_{AB}, x_{BE}, x_{EF} and a_2 are moved by the Newton–Raphson method until the four conditions are met at the three boundaries and the exit.

Regime III

The thinnest strips give rise to a local Hertzian-type pressure maximum near $x = 0$, as shown in Fig. 3c and by cases (e) and (f) of Fig. 1. In these cases the strip unloads elastically in zone C under the falling pressure. Two cases are distinguished: (1) the pressure peak near exit is higher than the Hertzian pressure maximum near $x = 0$ [case (e) of Fig. 1]; and (2) the pressure peak near exit is lower than the Hertzian maximum [case (f) of Fig. 1]. The simpler behaviour of case 1 will be considered and the details of case 2 omitted.

Assuming the strip thickness to be constant in the central no-slip regime (comprising the contained plastic zones B and D and the elastic no-slip zone C), the positions of the boundaries x_{BC} and x_{CD} have no influence on the pressure distribution $p(x)$. Hence $p(x)$ and boundaries x_{AB}, x_{DE}, x_{EF} and a_2 are found in an identical manner to that described for regime II. The boundaries x_{BC} and x_{CD} are located as follows.

In the no-slip zone B where the pressure is increasing, equation (12) shows that a small (contained) positive plastic strain rate $\dot{\varepsilon}_s^p$ is required to prevent the yield condition (3a) being violated. The contained plastic zone B ends when $\dot{\varepsilon}_s^p = 0$. Neglecting the small term in $J(x)$, equation (12) shows this to occur when $dp/dx = 0$, that is at the pressure maximum, which is taken to a good approximation as the location of the boundary x_{BC}. Elastic unloading follows the contained plastic zone and the stress in the strip $\sigma_x(x)$ is given by equation (14a). The elastic zone C continues until yield is again reached at the boundary x_{CD}, which by equation (14a) occurs when the pressure rises to its earlier maximum, that is $p(x_{CD}) = p(x_{BC})$. As before, the shear traction in the no-slip zones C and D is given by equation (36).

The nature of the solution in the central no-slip zone is more complex when $p(x_{EF})$ is less than $p(x_{BC})$. Fortunately, the pressure profile, strip thickness, rolling load and torque do not depend upon the detailed solution in the central no-slip zone, and there is no practical requirement to solve for the central zone. Admissible solutions have been found, but are not detailed here.

APPENDIX 3

The nature of the pressure peak in regimes II and III

In order to clarify the solution in the vicinity of the pressure peak at the end of the neutral zone in regimes II and III, an approximate analytical solution to the problem was developed by Greenwood *et al.* (**12**) using results from fracture mechanics.

The region in the location of the peak is modelled as shown in Fig. 11. For a peak located at x_p, the roll to the left of the peak [$\xi_1 \equiv (x_p - x) \geqslant 0$] is assumed to be deformed to a perfect flat [$v(\xi_1) = 0$] and that to the right of the peak ($\xi \equiv x_p - x \geqslant 0$) is subjected to a pressure $p(\xi)$ determined by the plastic deformation of the strip, that is by equation (15). The substitution

$$g(\xi) = p(\xi) - p_0\{a^2 - (x_p + \xi)^2\}^{1/2}$$

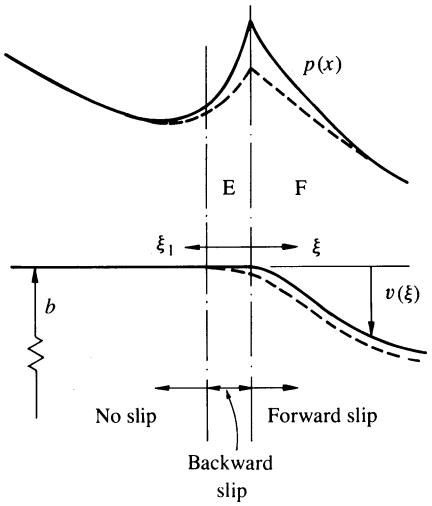

Fig. 11 Nature of solution at start of exit plastic zone
—— Perturbation solution via elastic fracture mechanics theory (assume $v = 0$ for $\xi_1 > 0$)
--- Full numerical solution ($v > 0$ in backward slip plastic zone E)

will be made, where $a = 2p_0 R/E_R^*$ and p_0 is the pressure at $x = 0$. It follows from the work of Barenblatt (**15**) and Schapery (**16**) that

$$p(\xi_1) = \frac{K}{\sqrt{(2\pi\xi_1)}} + g(O) + I\sqrt{(\xi_1)} + O(\xi_1) \tag{37}$$

and

$$v(\xi) = \frac{2}{\pi E_R^*} K\sqrt{(2\pi\xi)} - \frac{4}{3E_R^*} I\xi^{3/2} + O(\xi^2) \tag{38}$$

where

$$K = -\sqrt{\left(\frac{2}{\pi}\right)} \int_0^{\xi_2} \frac{g(\xi)}{\sqrt{\xi}}\, d\xi \tag{39}$$

and

$$I = \frac{2}{\pi} \int_0^{\xi_2} \frac{dg}{d\xi} \frac{1}{\sqrt{\xi}}\, d\xi \tag{40}$$

It is clear from equation (37) that the peak pressure at $\xi_1 = 0$ will be bounded and continuous if, and only if, $K = 0$; whereupon

$$p(\xi_1) = g(O) + I\sqrt{\xi_1} \tag{41}$$

and

$$v(\xi) = -\frac{4I}{3E_R^*} \xi^{3/2} \tag{42}$$

close to the peak, which shows that the deformed profile is smooth, with no discontinuity of gradient at the peak. However, the pressure gradient dp/ξ_1 given by equation (41) is singular at $\xi_1 = 0$ (see Fig. 11 and note that I is a negative quantity). The longitudinal stress σ_x must also be continuous and of value $p - Y_s$ at the peak, which leads to the conclusion that the pressure distribution of equation (41) causes yield adjacent to the peak. In order to satisfy the yield condition in this region it follows that there must be a small plastic reduction zone E to the left of the peak in which the strip is slipping *backwards* relative to the rolls. The peak has therefore the

characteristics of the classical 'friction hill' similar to cases (a) and (b) of Fig. 1. The peak thus coincides with a neutral section at which the direction of slip, and hence q, reverses (see Fig. 11).

The condition that $K = 0$ provides a relation which relates the position of the pressure peak x_p to the outlet position x_2. Using the approach outlined in this Appendix, Greenwood *et al.* (**12**) have obtained an approximate semi-analytical solution for pressure distribution $p(x)$ and deformed shape $b(x)$ which compares well with the complete numerical solutions (see Fig. 8).